On the stability of a loosely-coupled scheme based on a Robin interface condition for fluid-structure interaction

Giacomo Gigante[a], Christian Vergara[b,*]

[a] *Dipartimento di Ingegneria Gestionale, dell'Informazione e della Produzione, Università degli Studi di Bergamo, Italy,* giacomo.gigante@unibg.it

[b] *LABS, Dipartimento di Chimica, Materiali e Ingegneria Chimica "Giulio Natta", Politecnico di Milano, Italy,* christian.vergara@polimi.it

Abstract

We consider a loosely-coupled algorithm for fluid-structure interaction based on a Robin interface condition for the fluid problem (explicit Robin-Neumann scheme). We study the dependence of the stability of this method on the interface parameter in the Robin condition. In particular, for a model problem we find sufficient conditions for instability and stability of the method. In the latter case, we find a stability condition relating the time discretization parameter, the interface parameter, and the fluid and structure densities. Numerical experiments confirm the theoretical findings and highlight optimal choices of the interface parameter that guarantee accurate solutions.

Keywords: Fluid-structure interaction; loosely-coupled algorithms; Robin interface conditions; added mass effect

1. Introduction

Loosely-coupled schemes (also known as *explicit*) are a very attractive strategy for the numerical solution of the fluid-structure interaction (FSI) problem. Indeed, they are based on the solution of just one fluid and one structure problem at each time step, thus allowing a big improvement in the computational costs in comparison to fully-coupled (*implicit*) partitioned procedures and monolithic schemes. Another interesting feature of such schemes is that pre-existing fluid and structure solvers could be often employed.

For these reasons, loosely-coupled schemes have been widely used in many engineering applications such as aeroelasticity [28, 29, 13]. However, the stability properties of such schemes deteriorate when the so-called *added mass effect* becomes relevant. This may happen, in particular, when the fluid and structure densities are comparable, as happens in hemodynamics [31]. For example, in [10] it has been proven that the classical explicit *Dirichlet-Neumann* scheme is unconditionally unstable in the hemodynamic regime, see also [17, 27].

In the recent years, there has been a growing interest in partitioned procedures that are based on *Robin interface conditions*. The latter are obtained by considering linear combinations of the standard interface conditions owing to the introduction of suitable parameters. The choice of such parameters is crucial for accelerating the convergence of implicit schemes [3, 4, 2, 18, 19]. Some works focused then on the design of stable loosely-coupled schemes for scenarios which would feature large added mass effect with standard loosely-coupled schemes such as the explicit Dirichlet-Neumann one. Such schemes are based on Robin interface conditions [26, 20, 15, 14, 8, 7, 22, 6, 9]. These studies proposed specific values of the interface parameters which guarantee good stability properties (possibly in combination with suitable stabilizations).

In this paper, the explicit *Robin-Neumann* scheme, obtained by equipping the fluid subproblem with a Robin condition with parameter α and the structure one with a Neumann condition, is considered. In

*Corresponding author

Email addresses: giacomo.gigante@unibg.it (Giacomo Gigante), christian.vergara@polimi.it (Christian Vergara)

particular, it is investigated how the choice of the interface parameter α influences the stability of the numerical solution. To this aim, two analyses on a simplified problem, characterized by an inviscid fluid and a generalized string structure model, are performed, the first one determining sufficient conditions for instability of the scheme, whereas the second one sufficient conditions for its stability. This will allow us to understand the dependence of stability and instability on the physical and numerical parameters and to properly design stable loosely-coupled schemes which could be easily implemented also by means of available (even commercial) solvers.

This paper is organized as follows. In section 2 we present the model problem and its discretization. Section 3 reports the stability analysis in terms of the interface parameter and in Section 4 we present the results of some numerical experiments, where the issue of accuracy is also discussed by proposing some "optimal" value of the interface parameters.

2. Position of the problem

2.1. The fluid-structure interaction problem

We introduce in what follows the FSI model problem we have considered for the analyses reported below. This problem has been proposed in [10] and then used in other works, see e.g. [3, 11]. Although simple, this model problem allowed to obtain significant quantitiative indications about the convergence of iterative schemes or the stability of loosely-coupled methods. For example, in [10] the authors derived the well-known result about the stability of the explicit Dirichlet-Neumann scheme, providing an explicit constraint for the problem parameters. As it often happens in numerical analysis, the analysis of model problems (usually the only ones possible by analytical methods) allows to understand crucial numerical properties also related to more complex problems. For example, the stability result of [10] provided a mathematical explanation of the added mass effect and is at the basis of the motivation of why the explicit Dirichlet-Neumann scheme is not feasible in hemodynamics [31].

We consider the 2D fluid domain Ω^f which is a rectangle $R \times L$, where R is denoted the "radius" and L the length of the domain. Σ is the part where the interaction with the structure occurs, see Figure 1. For the fluid modeling, we consider a linear incompressible inviscid problem. For the structure modeling, we consider the 1D independent rings model [32] in the domain $\Omega^s = \Sigma$. The displacement can happen

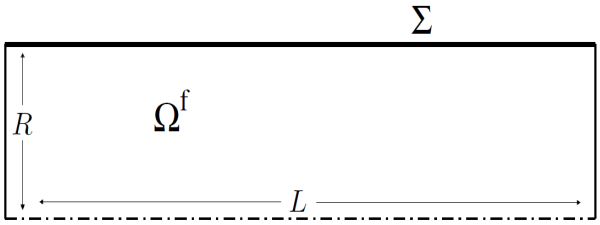

Figure 1: Fluid and structure domains for the simplified fluid-structure interaction problem.

only in the radial direction. Moreover, we assume small displacements so that the structure deformation is negligible and the fluid domain can be considered fixed. Thus, we have the following FSI problem:
Find the fluid velocity $\boldsymbol{u}$, the fluid pressure p, and the structure displacement η, such that

$$\rho_f \frac{\partial \boldsymbol{u}}{\partial t} + \nabla p = 0 \qquad \text{in } (0,T) \times \Omega^f, \tag{1a}$$

$$\nabla \cdot \boldsymbol{u} = 0 \qquad \text{in } (0,T) \times \Omega^f, \tag{1b}$$

$$\boldsymbol{u} \cdot \boldsymbol{n} = \frac{\partial \eta}{\partial t} \qquad \text{on } (0,T) \times \Sigma, \tag{1c}$$

$$\rho_s H_s \frac{\partial^2 \eta}{\partial t^2} + \beta \eta - \psi \frac{\partial^2 \eta}{\partial x^2} = p \qquad \text{on } (0,T) \times \Sigma, \tag{1d}$$

where $\boldsymbol{n}$ is the outward normal, ρ_f and ρ_s are the fluid and structure densities, x is the axial direction along which Σ is located, H_s is the structure thickness, and β and ψ are two suitable parameters accounting for the elasticity of the structure. Moreover, we have to equip the fluid problem with boundary conditions on $\partial\Omega^f \setminus \Sigma$, in particular pressure conditions imposing a pressure gradient between inlet and outlet, and an homogeneous Dirichlet condition on the lateral boundary, see [10]. Condition (1c) represents a no-slip condition at the interface Σ between the fluid and the structure (*perfect adherence* or *kinematic* condition). Due to the lower space dimension of the structure, the independent rings model (1d) represents also the third Newton law (continuity of the normal stresses or *dynamic* condition).

2.2. Time discretization and explicit Robin-Neumann scheme

Let Δt denote the time discretization parameter and $t^n = n\Delta t$ the discrete time instants for $n \geq 1$. Given a scalar- (resp. vector-) valued function of time $v(t)$ (resp. $\boldsymbol{v}(t)$), we denote by v^n (resp. $\boldsymbol{v}^n$) the approximation of $v(t^n)$ (resp. $\boldsymbol{v}(t^n)$) and we set $u^n = (\boldsymbol{u}^n \cdot \boldsymbol{n})|_\Sigma$. The discretized-in-time version of problem (25) at discrete time t^n reads: Find $\boldsymbol{u}^n$, p^n, and η^n, such that

$$\rho_f \frac{\boldsymbol{u}^n - \boldsymbol{u}^{n-1}}{\Delta t} + \nabla p^n = 0 \qquad \text{in } \Omega^f, \tag{2a}$$

$$\nabla \cdot \boldsymbol{u}^n = 0 \qquad \text{in } \Omega^f, \tag{2b}$$

$$u^n = \frac{\eta^n - \eta^{n-1}}{\Delta t} \qquad \text{on } \Sigma, \tag{2c}$$

$$\rho_s H_s \delta_{tt}\eta^n + \beta\eta^n - \psi\frac{\partial^2 \eta^n}{\partial x^2} = p^n \qquad \text{on } \Sigma. \tag{2d}$$

Notice that we have considered a backward Euler approximation for the fluid problem and we indicated with δ_{tt} the approximation of the second derivative in time for the structure problem, which will be specified later on.

By introducing the stability paramater $\alpha > 0$, we can substitute in (2) the kinematic condition (2c) with the following linear combination obtained with the dynamic condition (2d):

$$-\alpha u^n + p^n = -\alpha\frac{\eta^n - \eta^{n-1}}{\Delta t} + \rho_s H_s \delta_{tt}\eta^n + \beta\eta^n - \psi\frac{\partial^2 \eta^n}{\partial x^2} \quad \text{on } \Sigma. \tag{3}$$

Of course, the solution of problem (2a)-(2b)-(3)-(2d) coincides with that of (2).

We consider a partitioned strategy where condition (3) is given to the fluid problem, whereas (2d) is in fact the structure problem. Since the fluid problem has been discretized with an implicit method, in (3) we use the following implicit approximation of the second derivative:

$$\delta_{tt}\eta^n = \delta_{tt}^{Impl}\eta^n = \frac{\eta^n - 2\eta^{n-1} + \eta^{n-2}}{\Delta t^2}.$$

Instead, in the structure problem (2d) we use the explicit leap-frog approximation:

$$\delta_{tt}\eta^n = \delta_{tt}^{Expl}\eta^n = \frac{\eta^{n+1} - 2\eta^n + \eta^{n-1}}{\Delta t^2}.$$

We observe that, due to the explicit time discretization of the structure problem, the fluid and structure problems are in fact decoupled and, accordingly, we can introduce the following algorithm.

Algorithm 1. **Explicit Robin-Neumann algorithm.** Given $\boldsymbol{u}^0$, η^1, η^0, η^{-1}, for $n \geq 1$, at time step t^n:

1. Solve the fluid problem discretized in time by means of the implicit backward Euler method, with a Robin condition at the interface Σ:

$$\rho_f \frac{\boldsymbol{u}^n - \boldsymbol{u}^{n-1}}{\Delta t} + \nabla p^n = 0 \qquad \text{in } \Omega^f, \tag{4a}$$

$$\nabla \cdot \boldsymbol{u}^n = 0 \qquad \text{in } \Omega^f, \tag{4b}$$

$$-\alpha u^n + p^n = -\alpha \frac{\eta^n - \eta^{n-1}}{\Delta t} + \rho_s H_s \frac{\eta^n - 2\eta^{n-1} + \eta^{n-2}}{\Delta t^2} + \beta \eta^n - \psi \frac{\partial^2 \eta^n}{\partial x^2} \qquad \text{on } \Sigma; \tag{4c}$$

2. Solve the structure problem discretized in time by means of the explicit leap-frog method (coinciding with a Neumann condition at the interface Σ):

$$\rho_s H_s \frac{\eta^{n+1} - 2\eta^n + \eta^{n-1}}{\Delta t^2} + \beta \eta^n - \psi \frac{\partial^2 \eta^n}{\partial x^2} = p^n \quad \text{on } \Sigma; \tag{5}$$

3. Update the discrete time: $t^n \to t^{n+1}$.

Remark 2.1. Notice that both subproblems (4) and (5) are discretizations at time t^n. The fluid problem, due to the implicit discretization, is solved for u^n, whereas the structure problem, due to the explicit discretization, is solved for η^{n+1}. This allowed us to obtain a global explicit method, where just one fluid and one structure problem are solved at each time step.

Remark 2.2. The choice of an inviscid fluid is a simplification that allowed us to provide the analyses reported below and which has been already used in previous stability analyses, see e.g. [10]. In the numerical experiments reported in Section 4, we have considered a viscous fluid, due to the application we have in mind, i.e. hemodynamics. We believe that the choice of an inviscid fluid in the analyses could however provide meaningful stability results that could be used also for the viscous case. Indeed, the coupling between fluid and structure is mainly driven by the fluid pressure. For example, in [16] the authors showed that, in the framework of a Dirichlet-Neumann scheme, it is enough to strongly couple fluid pressure and structure displacement to have a stable scheme. This is also showed by our numerical results that confirmed all the theoretical findings, see Section 4.

In the next section, we study how the stability of Algorithm 1 is affected by the choice of the parameter α.

3. Stability analysis

3.1. Preliminaries

First, we notice that by using Algorithm 1, the discrete kinematic condition (2c) is not satisfied anymore. Indeed, from (5) we have

$$\beta \eta^n - \psi \frac{\partial^2 \eta^n}{\partial x^2} - p^n = -\rho_s H_s \frac{\eta^{n+1} - 2\eta^n + \eta^{n-1}}{\Delta t^2},$$

where it is understood from now on that the equations we derive hold true at the interface Σ. By introducing the latter expression in (4c), we obtain

$$-\alpha u^n = -\alpha \frac{\eta^n - \eta^{n-1}}{\Delta t} + \rho_s H_s \frac{\eta^n - 2\eta^{n-1} + \eta^{n-2}}{\Delta t^2} - \rho_s H_s \frac{\eta^{n+1} - 2\eta^n + \eta^{n-1}}{\Delta t^2},$$

which leads to

$$u^n = \frac{\eta^n - \eta^{n-1}}{\Delta t} + \rho_s H_s \frac{\eta^{n+1} - 3\eta^n + 3\eta^{n-1} - \eta^{n-2}}{\alpha \Delta t^2}. \tag{6}$$

The latter equation provides a "correction" of the discrete kinematic condition (2c) as a consequence of the explicit treatment.

Following [10], we consider the *added mass operator* $\mathcal{M} : H^{-1/2}(\Sigma) \to H^{1/2}(\Sigma)$, which allows us to write the following relation between fluid pressure and velocity at the interface, under the assumption of null external pressure:

$$p = -\rho_f \mathcal{M}\left(\frac{\partial(\boldsymbol{u}\cdot\boldsymbol{n})}{\partial t}\right) \quad \text{in } (0,T)\times\Sigma. \tag{7}$$

At the time discrete level, we have

$$p^n = -\rho_f \mathcal{M}\left(\frac{u^n - u^{n-1}}{\Delta t}\right).$$

Inserting (6) for both u^n and u^{n-1} in the previous equation, we obtain

$$p^n = -\rho_f \mathcal{M}\left(\frac{\eta^n - 2\eta^{n-1} + \eta^{n-2}}{\Delta t^2} + \frac{\rho_s H_s}{\alpha \Delta t^3}\left(\eta^{n+1} - 4\eta^n + 6\eta^{n-1} - 4\eta^{n-2} + \eta^{n-3}\right)\right), \tag{8}$$

which gives a relation between pressure and displacement at the interface.

We can write η^m for any $m \geq 1$ as a linear combination of the L^2 orthonormal basis functions $\left\{g_i(x) = \sqrt{2/L}\sin\left(\frac{i\pi x}{L}\right)\right\}$:

$$\eta^m(x) = \sum_{i=1}^{\infty} \eta_i^m g_i(x),$$

for suitable coefficients η_i^m, see [10, 3]. Notice that g_i are eigenfunctions of both the added mass operator $\mathcal{M}$ and of the Laplace operator $\mathcal{L} = -b\,\partial_{xx}|_\Sigma$, with eigenvalues given by

$$\mu_i = \frac{L}{i\pi \tanh\left(\frac{i\pi R}{L}\right)}, \quad \lambda_i = \left(\frac{i\pi}{L}\right)^2,$$

respectively.

It is useful for later purposes to highlight that the eigenvalues μ_i and λ_i of the discrete versions of the operators $\mathcal{M}$ and $\mathcal{L}$ obtained with a finite elements approximation, feature the following behaviours [10, 3]:

$$\mu_{min} \sim h, \qquad \lambda_{max} \sim h^{-2}, \qquad \mu_{max} \sim h^0, \tag{9}$$

where h is the space discretization parameter.

3.2. Sufficient conditions for instability

We present in what follows a first result that provides sufficient conditions that guarantee conditional instability of the explicit Robin-Neumann scheme. This result generalizes the one proven in [10] about the unconditional instability of the Dirichlet-Neumann scheme ($\alpha \to +\infty$, see Proposition 3 in [10]).

Proposition 1. The explicit Robin-Neumann scheme is unstable if

$$\rho_s H_s < \max_i \gamma_i, \quad \gamma_i = \alpha \Delta t \frac{4\rho_f \mu_i + \Delta t^2(\beta + \psi\lambda_i)}{16\rho_f \mu_i + 4\alpha\Delta t}. \tag{10}$$

Proof. We start by inserting in the interface condition (5) the expression of p^n given by (8), obtaining

$$\rho_s H_s \frac{\eta^{n+1} - 2\eta^n + \eta^{n-1}}{\Delta t^2} + \beta\eta^n - \psi\frac{\partial^2 \eta^n}{\partial x^2} +$$

$$\rho_f \mathcal{M}\left(\frac{\eta^n - 2\eta^{n-1} + \eta^{n-2}}{\Delta t^2} + \frac{\rho_s H_s}{\alpha\Delta t^3}\left(\eta^{n+1} - 4\eta^n + 6\eta^{n-1} - 4\eta^{n-2} + \eta^{n-3}\right)\right) = 0.$$

Notice that the previous is a relation in the discrete structure displacement solely. Multiplying it by the basis function g_i and integrating over the interface Σ, we obtain

$$\frac{\rho_s H_s}{\Delta t^2}\left(1+\frac{\rho_f\mu_i}{\alpha\Delta t}\right)\eta_i^{n+1}+\left(-\frac{2\rho_s H_s}{\Delta t^2}+\beta+\psi\lambda_i+\frac{\rho_f\mu_i}{\Delta t^2}-\frac{4\rho_s H_s\rho_f\mu_i}{\alpha\Delta t^3}\right)\eta_i^n+$$
$$\left(\frac{\rho_s H_s}{\Delta t^2}-2\frac{\rho_f\mu_i}{\Delta t^2}+\frac{6\rho_s H_s\rho_f\mu_i}{\alpha\Delta t^3}\right)\eta_i^{n-1}+\left(\frac{\rho_f\mu_i}{\Delta t^2}-\frac{4\rho_s H_s\rho_f\mu_i}{\alpha\Delta t^3}\right)\eta_i^{n-2}+\frac{\rho_s H_s\rho_f\mu_i}{\alpha\Delta t^3}\eta_i^{n-3}=0.$$

By multiplying the last identity by $\frac{\alpha\Delta t}{\rho_f\mu_i}$, we obtain the following characteristic polynomial corresponding to the previous difference equation:

$$\begin{aligned}\chi(y)= &\frac{\rho_s H_s}{\Delta t^2}\left(1+\frac{\alpha\Delta t}{\rho_f\mu_i}\right)y^4+\left(-\frac{2\alpha\rho_s H_s}{\rho_f\mu_i\Delta t}+\frac{\alpha\Delta t}{\rho_f\mu_i}(\beta+\psi\lambda_i)+\frac{\alpha}{\Delta t}-\frac{4\rho_s H_s}{\Delta t^2}\right)y^3\\ &+\left(\frac{\alpha\rho_s H_s}{\rho_f\mu_i\Delta t}-2\frac{\alpha}{\Delta t}+\frac{6\rho_s H_s}{\Delta t^2}\right)y^2+\left(\frac{\alpha}{\Delta t}-\frac{4\rho_s H_s}{\Delta t^2}\right)y+\frac{\rho_s H_s}{\Delta t^2}.\end{aligned}\tag{11}$$

Next, we compute the value of the previous polynomial for $y=-1$:

$$\begin{aligned}\chi(-1)&=\frac{16\rho_s H_s}{\Delta t^2}+\frac{4\alpha\rho_s H_s}{\rho_f\mu_i\Delta t}-\frac{4\alpha}{\Delta t}-\frac{\alpha\Delta t}{\rho_f\mu_i}(\beta+\psi\lambda_i)\\ &=\rho_s H_s\left(\frac{4\alpha}{\rho_f\mu_i\Delta t}+\frac{16}{\Delta t^2}\right)-\left(\frac{4\alpha}{\Delta t}+\frac{\alpha\Delta t(\beta+\psi\lambda_i)}{\rho_f\mu_i}\right).\end{aligned}$$

It follows that, under condition (10), $\chi(-1)<0$ for at least one value of i. Since $\lim_{y\to-\infty}\chi(y)=+\infty$, it follows that in this case there exists at least one real root $\bar{y}<-1$ of the polynomial associated to the difference equation, implying that the method is unstable. □

Remark 3.1. We notice that from the expression of γ_i in (10), this quantity blows up for $i\to\infty$. However, our interest will be that of analyzing the thesis of Proposition 1 in the discretized case, see Section 3.4 for further details.

3.3. Sufficient conditions for stability

We discuss in the following result some sufficient conditions that guarantee that the explicit Robin-Neumann scheme is conditionally stable. The idea is to start again from the polynomial (11) and discuss when its four roots have all modulus less than 1.

To this aim, we first introduce the following version of the implicit function theorem.

Theorem 3.2. *Let $f\in\mathcal{C}^1(\mathbb{R}^2)$ and suppose that for all $x\in\Omega$, an open interval, and for all*

$$y\in(\varphi_1(x),\varphi_2(x)),$$

where $\varphi_1,\varphi_2:\Omega\to\mathbb{R}$ are continuous functions, either

$$\frac{\partial f}{\partial y}(x,y)\geq b(x)>0\tag{12}$$

or

$$\frac{\partial f}{\partial y}(x,y)\leq b(x)<0,$$

for some continuous function $b:\Omega\to\mathbb{R}$ hold true. Let $g:\Omega\to\mathbb{R}$ be such that for all $x\in\Omega$

$$g(x)\in(\varphi_1(x),\varphi_2(x)),\tag{13a}$$

$$g(x)-\frac{f(x,g(x))}{b(x)}\in(\varphi_1(x),\varphi_2(x)).\tag{13b}$$

Then, there exists a unique function $\xi : \Omega \to \mathbb{R}$ *such that, for all* $x \in \Omega$, $\xi(x) \in (\varphi_1(x), \varphi_2(x))$ *and* $f(x, \xi(x)) = 0$. *Furthermore, for all* $x \in \Omega$

$$|\xi(x) - g(x)| \leq \left| \frac{f(x, g(x))}{b(x)} \right|.$$

Proof. Let us consider the case $\frac{\partial f}{\partial y}(x, y) \geq b(x) > 0$. The other case follows from it after replacing $f(x, y)$ with $-f(x, y)$ and $b(x)$ with $-b(x)$. Fix $x \in \Omega$. By strict monotonicity of the function $y \mapsto f(x, y)$ in the interval $(\varphi_1(x), \varphi_2(x))$, there exists at most one value $\xi(x) \in (\varphi_1(x), \varphi_2(x))$ for which $f(x, \xi(x)) = 0$. This proves uniqueness.

The function $y \mapsto f(x, y)$ takes the value $f(x, g(x))$ at $y_0 = g(x)$. Next, consider the point

$$y_1 = y_0 - \frac{f(x, y_0)}{b(x)},$$

and assume without loss of generality that $y_0 \leq y_1$, that is $f(x, y_0) \leq 0$. By the hypotheses, it holds $[y_0, y_1] \subseteq (\varphi_1(x), \varphi_2(x))$, so that for all $y \in [y_0, y_1]$ it holds $\frac{\partial f}{\partial y}(x, y) \geq b(x) > 0$ and

$$\begin{aligned} f(x, y_1) &= \int_{y_0}^{y_1} \frac{\partial f}{\partial y}(x, t)\, dt + f(x, y_0) \\ &\geq b(x)(y_1 - y_0) + f(x, y_0) \\ &= b(x)\left(y_0 - \frac{f(x, y_0)}{b(x)} - y_0 \right) + f(x, y_0) = 0. \end{aligned}$$

By the intermediate value theorem, there exists a point $\xi(x) \in [y_0, y_1]$ such that $f(x, \xi(x)) = 0$. This proves existence.

Finally,

$$y_0 \leq \xi(x) \leq y_1$$

means

$$g(x) \leq \xi(x) \leq g(x) - \frac{f(x, g(x))}{b(x)}$$

so that

$$|\xi(x) - g(x)| \leq \left| \frac{f(x, g(x))}{b(x)} \right|,$$

proving the last part of the theorem. □

We are ready to introduce the main result of this work.

Theorem 3.3. *For all positive* ρ_s, ρ_f, α, H_s *and for all finite sequences of positive eigenvalues* $\{\mu_i\}_{i=1}^N$, $\{\lambda_i\}_{i=1}^N$, *there exists a positive* δ *such that, if* $0 < \Delta t < \delta$, *then, for all* $i = 1, \ldots, N$, *the polynomial* (11) *has four simple roots in the open unit disc in the complex plane.*

Proof. It is convenient to normalize $\chi(y)$, setting

$$\begin{aligned} Q(y) &= \frac{\Delta t^2}{\rho_s H_s} \chi(y) \\ &= (1 + B_i z) y^4 - \left(4 + (2B_i - A) z - AC_i z^3\right) y^3 + (6 + (B_i - 2A) z) y^2 \\ &\quad - (4 - Az) y + 1, \end{aligned}$$

where

$$\begin{aligned} z &= \Delta t > 0, \\ A &= \frac{\alpha}{\rho_s H_s} > 0, \\ B_i &= \frac{\alpha}{\rho_f \mu_i} > 0, \\ C_i &= \frac{1}{\rho_f \mu_i} (\beta + \psi \lambda_i) > 0. \end{aligned}$$

For technical reasons, we will equivalently study the polynomial

$$\begin{aligned} P(x) &= x^4 Q\left(\frac{1}{x}\right) \\ &= x^4 - (4 - Az) x^3 + (6 + (B_i - 2A) z) x^2 \\ &\quad - \left(4 + (2B_i - A) z - AC_i z^3\right) x + (1 + B_i z), \end{aligned} \tag{14}$$

showing that all its four roots have modulus greater than 1. Observe first that when $z = 0$, $P(x)$ reduces to

$$x^4 - 4x^3 + 6x^2 - 4x + 1 = (x - 1)^4.$$

By classical results, this implies that for sufficiently small z, $P(x)$ has four simple roots as close as desired to $x = 1$ in the complex plane (see [21], page 122). Unfortunately, this is not sufficient for our purposes, and for this reason we need a deeper analysis.

Next, set $x = 1 + U$. This simplifies our formulas, since we look for roots that are close to 1. This gives

$$P(1 + U) = U^4 + AzU^3 + (B_i + A) zU^2 + AC_i z^3 U + AC_i z^3. \tag{15}$$

Recalling that U is a complex variable, we write it as $U = u + iv$ where u and v are its real and imaginary parts, respectively. Thus, the equation

$$(u + iv)^4 + Az(u + iv)^3 + (B_i + A) z(u + iv)^2 + AC_i z^3 (u + iv) + AC_i z^3 = 0$$

reduces to the system

$$\begin{cases} v^4 - v^2 \left(6u^2 + 3Azu + z(A + B_i)\right) + u^4 + Azu^3 + (A + B_i) zu^2 \\ \qquad + AC_i z^3 u + AC_i z^3 = 0, \\ v\left(-v^2 (4u + Az) + 4u^3 + 3Au^2 z + 2uz(A + B_i) + AC_i z^3\right) = 0. \end{cases} \tag{16}$$

Notice that the solution of the second equation $v = 0$ reduces the first equation to

$$u^4 + (u + 1) Azu^2 + B_i zu^2 + AC_i z^3 (u + 1) = 0,$$

which does not have any real solution $u > -1$ (all summands are positive). Since we look for roots $u + iv$ close to 0, we disregard the solution of the second equation $v = 0$ and focus on the other solution

$$v^2 = \frac{4u^3 + 3Au^2 z + 2uz(A + B_i) + AC_i z^3}{4u + Az}, \tag{17}$$

which reduces the first equation to

$$T_6 u^6 + T_5 u^5 + T_4 u^4 + T_3 u^3 + T_2 u^2 + T_1 u + T_0 = 0, \tag{18}$$

where

$$
\begin{aligned}
T_6 &= -64, \\
T_5 &= -96Az, \\
T_4 &= 32\left(A+B_i\right)z + 48A^2z^2, \\
T_3 &= 32A\left(A+B_i\right)z^2 + 8A^3z^3, \\
T_2 &= 4\left(A+B_i\right)^2z^2 + 8A\left(A^2+B_iA-2C_i\right)z^3 + 4A^2C_iz^4, \\
T_1 &= -2A\left(A+B_i\right)^2z^3 + 8A^2C_iz^4 - 2A^3C_iz^5, \\
T_0 &= -A^2C_i\left(B_i - zC_i\right)z^5.
\end{aligned}
$$

Since we look for roots that go to 0 with z, we may assume that u is $O\left(z\right)$ as $z \to 0$. The original equation (18) can therefore be approximated with

$$T_2u^2 + T_1u + T_0 = 0;$$

further, disregarding all higher order terms in z, it can be approximated with

$$4\left(A+B_i\right)^2u^2 - 2A\left(A+B_i\right)^2zu - A^2z^3C_iB_i = 0. \tag{19}$$

If $u = O\left(z\right)$, then the third term in the above equation can be neglected and the same equation can be approximated with

$$4u - 2Az = 0,$$

which gives the approximate solution

$$u = \frac{A}{2}z.$$

If $u = O\left(z^2\right)$, then the first term in equation (19) can be neglected and (19) can be approximated with

$$2\left(A+B_i\right)^2u + Az^2C_iB_i = 0,$$

which gives the approximate solution

$$u = -\frac{AC_iB_i}{2\left(A+B_i\right)^2}z^2.$$

Next, we need to estimate the derivative with respect to u of

$$f\left(z,u\right) = T_6u^6 + T_5u^5 + T_4u^4 + T_3u^3 + T_2u^2 + T_1u + T_0,$$

that is

$$\frac{\partial f}{\partial u}\left(z,u\right) = 6T_6u^5 + 5T_5u^4 + 4T_4u^3 + 3T_3u^2 + 2T_2u + T_1. \tag{20}$$

We are ready to apply Theorem 3.2, with the two following choices for g suggested by the previous approximate solutions:

$$
\begin{aligned}
g_1(z) &= \frac{A}{2}z, \\
g_2(z) &= -\frac{AC_iB_i}{2\left(A+B_i\right)^2}z^2.
\end{aligned}
$$

Assume first u close to $g_1\left(z\right)$. Precisely, assume that for some $K_1 > 0$, $\varphi_1\left(z\right) = g_1\left(z\right) - K_1z^2 \leq u \leq \varphi_2\left(z\right) = g_1\left(z\right) + K_1z^2$, so that hypothesis (13a) in Theorem 3.2 is satisfied. In particular, $u = g_1\left(z\right) + O\left(z^2\right)$

and, from (20),

$$\begin{aligned}\frac{\partial f}{\partial u}(z,u) &= 8(A+B_i)^2 z^2 u - 2A(A+B_i)^2 z^3 + O\left(z^4\right)\\ &= 8(A+B_i)^2 z^2 g_1(z) - 2A(A+B_i)^2 z^3 + O\left(z^4\right)\\ &= 2A(A+B_i)^2 z^3 + O\left(z^4\right).\end{aligned}$$

Thus, for some small positive δ_1, if $0 < z < \delta_1$ and $g_1(z) - K_1 z^2 \le u \le g_1(z) + K_1 z^2$, it holds

$$\frac{\partial f}{\partial u}(z,u) \ge A(A+B_i)^2 z^3 = b_1(z),$$

which shows that, with the above choices, hypothesis (12) in Theorem 3.2 is satisfied.

Next, we need to check hypothesis (13b) in Theorem 3.2, that is

$$g_1(z) - K_1 z^2 \le g_1(z) - \frac{f(z, g_1(z))}{b_1(z)} \le g_1(z) + K_1 z^2,$$

or, in other words,

$$\frac{f(z, g_1(z))}{b_1(z)} = O\left(z^2\right).$$

It holds:

$$\begin{aligned}\frac{f(z, g_1(z))}{b_1(z)} &= \frac{4(A+B_i)^2 z^2 g_1(z)^2 - 2A(A+B_i)^2 z^3 g_1(z) + O\left(z^5\right)}{A(A+B_i)^2 z^3}\\ &= \frac{(A+B_i)^2 z^2 A^2 z^2 - A(A+B_i)^2 z^3 A z + O\left(z^5\right)}{A(A+B_i)^2 z^3}\\ &= O\left(z^2\right),\end{aligned}$$

since the first two terms at numerator vanish. Thus, it follows from Theorem 3.2 that there exists a unique function

$$u_1 : (0, \delta_1) \to \left(\frac{A}{2} z - K_1 z^2, \frac{A}{2} z + K_1 z^2\right)$$

such that $f(z, u_1(z)) = 0$ for all $z \in (0, \delta_1)$. Furthermore, for all $z \in (0, \delta_1)$

$$\left| u_1(z) - \frac{A}{2} z \right| \le \frac{f(z, g_1(z))}{b_1(z)},$$

which implies that

$$u_1(z) = \frac{A}{2} z + O\left(z^2\right)$$

as $z \to 0^+$.

Similarly, let us assume u close to $g_2(z)$. Precisely, assume that for some $K_2 > 0$, $\psi_1(z) = g_2(z) - K_2 z^3 \le u \le \psi_2(z) = g_2(z) + K_1 z^3$. Then, it holds $u = g_2(z) + O\left(z^3\right)$ and

$$\frac{\partial f}{\partial u}(z,u) = -2A(A+B_i)^2 z^3 + O\left(z^4\right).$$

Thus, for some small positive δ_2, if $0 < z < \delta_2$ and $g_2(z) - K_2 z^3 \le u \le g_2(z) + K_2 z^3$, it holds

$$\frac{\partial f}{\partial u}(z,u) \le -A(A+B_i)^2 z^3 = b_2(z).$$

Next, we need to check if

$$g_2(z) - K_2 z^3 \leq g_2(z) - \frac{f(z, g_2(z))}{b_2(z)} \leq g_2(z) + K_2 z^3$$

or, in other words, if

$$\frac{f(z, g_2(z))}{b_2(z)} = O\left(z^3\right).$$

It holds:

$$\begin{aligned}
\frac{f(z, g_2(z))}{b_2(z)} &= \frac{-2A(A+B_i)^2 z^3 g_2(z) - A^2 z^5 C_i B_i + O\left(z^6\right)}{-A(A+B_i)^2 z^3} \\
&= \frac{z^3 A^2 C_i B_i z^2 - A^2 z^5 C_i B_i + O\left(z^6\right)}{A(A+B_i)^2 z^3} \\
&= O\left(z^3\right).
\end{aligned}$$

Thus, it follows from Theorem 3.2 that there exists a unique function

$$u_2 : (0, \delta_2) \to \left(-\frac{AC_i B_i}{2(A+B_i)^2} z^2 - K_2 z^3, -\frac{AC_i B_i}{2(A+B_i)^2} z^2 + K_2 z^3 \right)$$

such that $f(z, u_2(z)) = 0$ for all $z \in (0, \delta_2)$. Furthermore, for all $z \in (0, \delta_2)$

$$\left| u_2(z) + \frac{AC_i B_i}{2(A+B_i)^2} z^2 \right| \leq \frac{f(z, g_2(z))}{b_2(z)},$$

which implies that

$$u_2(z) = -\frac{AC_i B_i}{2(A+B_i)^2} z^2 + O\left(z^3\right)$$

as $z \to 0^+$.

Let us compute v^2 by means of (17) for these two choices. Setting $u = u_1(z) = \frac{A}{2} z + O\left(z^2\right)$, we obtain

$$\begin{aligned}
v_1^2 &= \frac{4u_1^3 + 3Au_1^2 z + 2u_1 z(A+B_i) + AC_i z^3}{4u_1 + Az} \\
&= \frac{Az^2(A+B_i) + O\left(z^3\right)}{3Az + O\left(z^2\right)} \\
&= \frac{(A+B_i)}{3} z + O\left(z^2\right).
\end{aligned}$$

Setting $u = u_2(z) = -\frac{AC_i B_i}{2(A+B_i)^2} z^2 + O\left(z^3\right)$, we obtain

$$\begin{aligned}
v_2^2 &= \frac{4u_2^3 + 3Au_2^2 z + 2u_2 z(A+B_i) + AC_i z^3}{4u_2 + Az} \\
&= \frac{2z(A+B_i)\left(-\frac{AC_i B_i}{2(A+B_i)^2} z^2\right) + AC_i z^3 + O\left(z^4\right)}{Az + O\left(z^2\right)} \\
&= \frac{\frac{AC_i A}{A+B_i} z^3 + O\left(z^4\right)}{Az + O\left(z^2\right)} \\
&= \frac{C_i A}{A+B_i} z^2 + O\left(z^3\right).
\end{aligned}$$

Thus, (u_1, v_1) and (u_2, v_2) are solutions of system (16). This means that $u_1 \pm iv_1$ and $u_2 \pm iv_2$ are the 4 roots of (15) and $1 + u_1 \pm iv_1$ and $1 + u_2 \pm iv_2$ are the four roots of (14).

The final step of the proof is to show that these four roots for $P(x)$ have modulus greater than 1. Accordingly, it holds

$$(1+u_1)^2 + v_1^2 = 1 + Az + \frac{(A+B_i)}{3} z + O\left(z^2\right), \quad \text{as } z \to 0^+.$$

Thus, there exists a positive δ_3 such that $(1+u_1)^2 + v_1^2 > 1$ for $z < \delta_3$. Moreover, it holds

$$\begin{aligned}
(1+u_2)^2 + v_2^2 &= \left(1 - \frac{AC_iB_i}{2\left(A+B_i\right)^2} z^2\right)^2 + \frac{C_iA}{(A+B_i)} z^2 + O\left(z^3\right) \\
&= 1 - \frac{AC_iB_i}{\left(A+B_i\right)^2} z^2 + \frac{C_iA}{(A+B_i)} z^2 + O\left(z^3\right) \\
&= 1 + \frac{C_iA^2}{\left(A+B_i\right)^2} z^2 + O\left(z^3\right), \quad \text{as } z \to 0^+.
\end{aligned}$$

Thus, there exists a positive δ_4 such that $(1+u_2)^2 + v_2^2 > 1$ for $z < \delta_4$.

This proves that the four roots of $\chi(y)$ in (11) have all modulus strictly less than 1, provided that $\Delta t < \delta = \min\{\delta_1, \delta_2, \delta_3, \delta_4\}$.

□

Remark 3.4. We observe that δ in the previous theorem depends on ρ_s, ρ_f, α, H_s, $\mu_i\,\lambda_i$. However, since such values are fixed for a given specific problem, we were able to prove the stability of the method provided that Δt is small enough.

3.4. Discussion on the stability and instability conditions

The results proven above give us sufficient conditions for instability or stability of the explicit Robin-Neumann scheme. In particular, in the last case, we found that, given $\alpha > 0$, for Δt small enough this scheme is absolutely stable.

In view of the numerical experiments, we discuss hereafter more in detail the hypotheses of the previous results in the discretized case, that is considering eigenvalues λ_i and μ_i in a range of interest characterized by the relevant frequencies induced by the introduction of the computational mesh, see in particular (9). To this aim, in what follows we propose three (non equivalent) sufficient conditions that imply the instability condition (10):

i)

$$\rho_s H_s < \alpha \Delta t \frac{4\rho_f \mu_{\min} + \Delta t^2 \left(\beta + \psi \lambda_{\max}\right)}{16\rho_f \mu_{\min} + 4\alpha \Delta t} = \overline{\eta}. \tag{21}$$

This is obtained by taking the greatest possible value of i in (10);

ii)

$$\begin{cases} \rho_s H_s < \rho_f \mu_{\min} + \Delta t^2 \left(\beta + \psi \lambda_{\max}\right)/4 = \eta_1 \\ \\ \alpha > \dfrac{16\rho_f \mu_{\min} \rho_s H_s}{\Delta t \left(4\rho_f \mu_{\min} + \Delta t^2 \left(\beta + \psi \lambda_{\max}\right) - 4\rho_s H_s\right)} = \alpha_1. \end{cases} \tag{22}$$

This is obtained by solving (21) in the variable α;

iii)

$$\begin{cases} \rho_s H_s < \rho_f \mu_1 = \eta_2 \\ \\ \alpha > \dfrac{4\rho_f \mu_1 \rho_s H_s}{\Delta t \left(\rho_f \mu_1 - \rho_s H_s\right)} = \alpha_2. \end{cases} \tag{23}$$

This is obtained by taking $i = 1$ in (10), deleting the term $\Delta t^2 (\beta + \psi \lambda_1)$ and solving in α.

1. **Dependence on $\rho_s H_s$.** By looking at conditions (22) and (23), we see that when $\rho_s H_s < \max(\eta_1, \eta_2)$, the explicit Robin-Neumann scheme is unstable if α is large enough. In particular, for decreasing values of $\rho_s H_s < \eta_1$ (i.e. for scenarios where the added mass effect would increase if the explicit Dirichlet-Neumann scheme was used), the value of α_1 decreases, enlarging the range of α such that the scheme is unstable. The same argument holds true for α_2 when $\rho_s H_s < \eta_2$.

2. **Dependence on Δt.** From Theorem 3.3, it holds that for any fixed $\alpha > 0$, the explicit Robin-Neumann scheme is stable provided that Δt is small enough. This result is consistent with Proposition 1. Indeed, for all indices i, it holds

$$\lim_{\Delta t \to 0} \gamma_i = \lim_{\Delta t \to 0} \alpha \Delta t \frac{4\rho_f \mu_i + \Delta t^2 (\beta + \psi \lambda_i)}{16 \rho_f \mu_i + 4\alpha \Delta t} = 0.$$

   Accordingly, it holds also from (22):

$$\lim_{\Delta t \to 0} \alpha_1 = +\infty.$$

   Observe also that, by (23), for $\rho_s H_s < \eta_2$ instability of the scheme follows if

$$\Delta t > \frac{4\rho_f \mu_1 \rho_s H_s}{\alpha \left(\rho_f \mu_1 - \rho_s H_s\right)}.$$

   This means that in order to have stability according to Theorem 3.3 we need at least $\delta \leq c\alpha^{-1}$. The dependence of δ on α is still under study and will be hopefully discussed in future studies.

3. **Dependence on h.** By exploiting the behaviour of μ_{min} and λ_{max} with respect to h, see (9), we find from (21) that $\lim_{h \to 0} \overline{\eta} = +\infty$ for Δt fixed. This means that the stability properties of the method deteriorates when h decreases. This is justified by the fact that when h becomes small, the fluid and structure solutions should match a larger number of d.o.f. at the interface and, due to the implicit treatment for the fluid time discretization and the explicit one for the structure, this matching becomes more and more difficult to be satisfied for decreasing values of h.

4. **$\boldsymbol{\Delta t, h \to 0}$.** From (9) and (22), it holds that if $\Delta t \sim h$, then $\lim_{\Delta t, h \to 0} \alpha_1 \simeq \frac{16 \rho_s H_s \rho_f}{\psi - 4\rho_s H_s}$. When $\rho_s H_s$ is small enough (i.e. in presence of large added mass effect if the explicit Dirichlet-Neumann scheme was used), this limit is positive and bounded, unlike the case $\Delta t \to 0, h$ fixed (cf. point 2). This means that in this case we have instability for a wide range of values of α even as $\Delta t \to 0$. This suggests that the value of δ in Theorem 3.3 should be smaller (up to a constant) than h. Indeed, we have the following result.

   Lemma 3.5. *The value of δ in Theorem 3.3 satisfies the relation*

$$\delta < ch,$$

   for a suitable constant c.

   Proof. Fix $\alpha > 0$. Call $\delta = f(h)$ the relationship between δ and h. Let assume that the thesis is not true, that is that there exists a sequence of values h_j and correspondingly $\delta_j = f(h_j)$, such that

$$\lim_{j \to +\infty} \frac{\delta_j}{h_j} = +\infty. \tag{24}$$

From Theorem 3.3, it holds that stability is guaranteed if $\Delta t = \Delta t_j = \delta_j/2$. On the other side, from (24) and the choice of Δt above, it holds $h_j = o(\delta_j) = o(\Delta t_j)$. From (21), it holds that in the range $h = o(\Delta t)$, $\lim_{\Delta t, h\to 0} \overline{\eta} = +\infty$, obtaining unconditional instability. This contradicts the previous finding about stability. This means that the thesis is true. □

5. **The cases $\alpha = +\infty$ and $\alpha = 0$.** Theorem 3.3 holds true for any $\alpha \in (0, +\infty)$. The case $\alpha = +\infty$ corresponds to the explicit Dirichlet-Neumann scheme. In this case, the polynomial $\chi(y)$ in (11) corresponds to the one found in [10] (see Proposition 3 therein), where it is shown that at least one root has modulus greater than one independently of Δt (cf. also (21)).

   Regarding $\alpha = 0$, we obtain $\chi(y) = \frac{\rho_s H_s}{\Delta t^2}(y-1)^4$. This means that the solution does not blow up, even if it is not strictly absolute stable. This is in accordance with the fact that in this case the numerical solution does not evolve during the time evolution, being always equal to the initial condition (the same Neumann datum is transferred at the interface). Thus, accuracy is completely lost. From this observation, we can argue that too small values of α, even though give stability, do not lead to an accurate solution.

4. Numerical results

4.1. Preliminaries

In this section we present some numerical results with the aim of validating the theoretical findings reported in the previous section. In particular, we studied the effectiveness of the analyses obtained for the model problem (25), when applied to complete three-dimensional fluid and structure models. Indeed, the analysis, although performed over a simplified model, might give important indications about the stability of the explicit Robin-Neumann scheme also in more complex scenarios. This is a quite common attitude, see for example [10, 3, 11] which used the same simplified model for the analysis and then investigated the effectiveness of their findings in more complex numerical experiments.

All the simulations are inspired from hemodynamics. This problem is of great interest for our purposes since it is in general characterized by a large added mass effect, so that the stability of explicit methods is a challenging issue.

We considered in particular a 3D incompressible fluid described by the Navier-Stokes equations written in the Arbitrary Lagrangian-Eulerian formulation [12] and a 3D linear elastic structure. Ω_f and Ω_s are the fluid and structure domains, Σ the fluid-structure interface, Σ^{out} the external structure surface, $\boldsymbol{n}$ the unit normal outgoing the fluid domain, and $\boldsymbol{n}_s$ the unit normal outgoing the structure domain. Then, for each t, we have [30]:

$$\rho_f \partial_t^A \boldsymbol{u} + \rho_f((\boldsymbol{u}-\boldsymbol{w})\cdot\nabla)\boldsymbol{u} - \nabla\cdot\boldsymbol{T}_f(\boldsymbol{u},p) = \boldsymbol{0} \quad \text{in } \Omega_f, \tag{25a}$$

$$\nabla\cdot\boldsymbol{u} = 0 \quad \text{in } \Omega_f, \tag{25b}$$

$$\boldsymbol{u} = \partial_t\boldsymbol{\eta} \quad \text{on } \Sigma, \tag{25c}$$

$$\boldsymbol{T}_f\boldsymbol{n} = \boldsymbol{T}_s\boldsymbol{n} \quad \text{on } \Sigma, \tag{25d}$$

$$\rho_s\partial_{tt}\widehat{\boldsymbol{\eta}} - \nabla\cdot\widehat{\boldsymbol{T}}_s(\widehat{\boldsymbol{\eta}}) = \boldsymbol{0} \quad \text{in } \widehat{\Omega}_s, \tag{25e}$$

$$\gamma_{ST}\widehat{\boldsymbol{\eta}} + \widehat{\boldsymbol{T}}_s(\widehat{\boldsymbol{\eta}})\boldsymbol{n}_s = 0 \quad \text{on } \widehat{\Sigma}^{out}, \tag{25f}$$

where $\boldsymbol{T}_f(\boldsymbol{u},p) = -p\boldsymbol{I} + \mu(\nabla\boldsymbol{u} + (\nabla\boldsymbol{u})^T)$ is the fluid Cauchy stress tensor and μ the dynamic viscosity; ∂_t^A is the ALE time derivative and $\boldsymbol{w}$ is the velocity of the fluid domain obtained by solving an harmonic extension of the interface structure velocity with homogeneous Dirichlet boundary conditions on $\partial\Omega_f \setminus \Sigma$. The structure problem (25e) is instead solved in a Lagrangian framework, identified by $\widehat{\ }$. Moreover, $\boldsymbol{T}_s$ is the structure Cauchy stress tensor given by

$$\boldsymbol{T}_s(\boldsymbol{\eta}) = \tfrac{E}{2(1+\nu)}(\nabla\boldsymbol{\eta} + (\nabla\boldsymbol{\eta})^T) + \tfrac{\nu E}{(1+\nu)(1-2\nu)}(\nabla\cdot\boldsymbol{\eta})\boldsymbol{I},$$

where E is the Young modulus E and ν the Poisson ratio. Condition at the external surface (25f) represents a Robin condition to account for the effect of an elastic surrounding tissue with elasticity modulus γ_{ST} [23]. The previous problem needs to be completed with boundary and initial conditions.

For the time discretization, we used the same BDF schemes of the analysis for both the fluid and structure, with a semi-implicit treatment of the fluid convective term, whereas for the space discretization we employed $P1bubble - P1$ finite elements for the fluid and $P1$ finite elements for the structure. The fluid domain at each time step is obtained by extrapolation of previous time steps (semi-implicit approach [16, 5, 25]). We used the following data: fluid viscosity $\mu = 0.035\, g/(cm\, s)$, fluid density $\rho_f = 1\, g/cm^3$, structure density $\rho_s = 1.1\, g/cm^3$, Poisson ratio $\nu = 0.49$, Young modulus $E = 3 \cdot 10^5\, Pa$, surrounding tissue parameter for the structure problem [23] $\gamma_{ST} = 1.5 \cdot 10^5\, Pa/cm$.

The fluid domain is a cylinder with length $L = 5\, cm$ and radius $R = 0.5\, cm$, whereas the structure domain is the external cylindrical crown with thickness $H_s = 0.1\, cm$. The thickness of the structure is small enough to make acceptable the use of a membrane model in the stability analysis of model problem (25). We considered a couple of meshes with 4680 tetrahedra and 1050 vertices for the fluid and 1260 vertices for the structure (mesh I). Another couple of meshes (mesh II) has been obtained by halving the values of the space discretization parameter.

In all the cases we reported also the numerical solution obtained with the same Δt by using an implicit method, in particular the Robin-Neumann scheme, with an absolute tolerance of 10^{-7} on the convergence of the interface conditions. In these cases, the value of α has been set by following the optimization procedure proposed in [19] for the Robin-Robin scheme in the case of cylindrical interfaces. This leads to two optimal values α_f^{opt} and α_s^{opt} in the Robin interface conditions. Since in the hemodynamic regime the convergence properties of the implicit Robin-Neumann scheme with the optimal value α_f^{opt} are very similar to that of the "optimal" implicit Robin-Robin scheme [18], we propose here to use $\alpha = \alpha_f^{opt}$ for the implicit Robin-Neumann scheme. In Table 1 we reported the values of such optimal values α_f^{opt} for different Δt and for mesh I.

Δt	α_f^{opt}
10^{-3}	1702
$5 \cdot 10^{-4}$	1045
$2.5 \cdot 10^{-4}$	866
$1.25 \cdot 10^{-4}$	857
$6.25 \cdot 10^{-5}$	900
$3.125 \cdot 10^{-5}$	1034

Table 1: Values of the optimal parameter α_f^{opt} obtained to accelerate the implicit RN scheme.

If not otherwise specified, at the inlet we prescribed a Neumann condition given by the following pressure function

$$P_{in} = 500 \left(1 - \cos\left(\frac{2\pi t}{0.01}\right)\right)\ dyne/cm^2, \quad t \le T = 0.04\, s,$$

with absorbing resistance conditions at the outlets [26, 24].

All the numerical results have been obtained with the parallel Finite Element library `LIFEV` [1].

4.2. On the stability of the numerical solution

In the first set of numerical experiments, we study the stability of the solution obtained by means of the explicit Robin-Neumann scheme. The time discretization parameter is $\Delta t = 0.0005\, s$. In Figure 2 we report the mean pressure over the middle cross section of the cylinder obtained for different values of α and with the RN implicit method.

From these results we observe stability of the numerical solution obtained with the explicit Robin-Neumann method for some values of the interface parameter α. The accuracy deteriorates for values of α

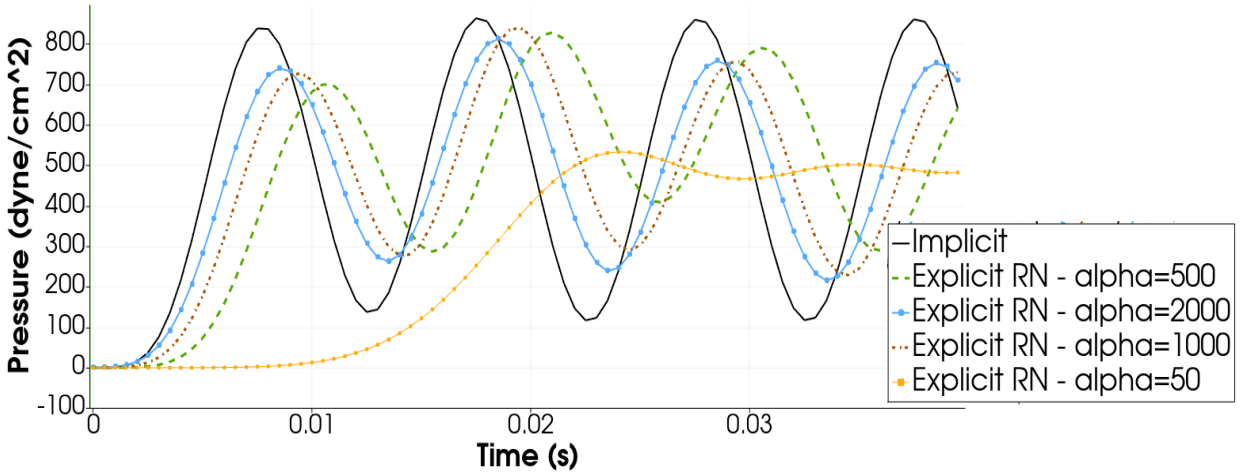

Figure 2: Fluid mean pressure over the middle cross section ($z = L/2 = 2.5\,cm$) for different values of α. In black the solution obtained with an implicit method.

approaching 0 (cf. point 5 in the Discussion of Sect. 3.4). Notice also that with $\alpha = 2500$ the numerical solution (not reported here) blows up. The same happens for bigger values of α. This is consistent with the result proven in Proposition 1, for which an unstable solution is obtained for α greater than a threshold when the ratio between fluid and structure densities is large enough, see (22)-(23) (cf. also point 1 in the Discussion of Sect. 3.4).

In Table 2 we indicate if stability is achieved for different space and time discretizations parameters. From the first two rows, we observe that, given a value of α, stability is achieved only if Δt is small enough.

Mesh	Δt	α	Stability
I	$0.625 \cdot 10^{-4}$	4689	OK
I	$1.25 \cdot 10^{-4}$	4689	NO
I	$1.25 \cdot 10^{-4}$	2000	OK
I	$5 \cdot 10^{-4}$	2000	OK
II	$5 \cdot 10^{-4}$	2000	NO

Table 2: Stability of the explicit RN scheme for different values of the parameters.

Indeed, with the greatest Δt no stability is achieved and the numerical solution blows up. This was expected from the theoretical findings, cf. Theorem 3.3, Remark 3.4 and point 2 in the Discussion of Sect. 3.4. From the first three lines, we observe that the value of Δt needed to have stability could be increased when α is decreased. This is in accordance with point 2 in the Discussion of Sect. 3.4. Finally, from the last two rows, we find that stability is achieved for given values of α and Δt if the mesh is not too fine. Indeed, with the finest mesh (mesh II) no stability is achieved and the numerical solution blows up. Again, this confirms the observation made in the Discussion of Sect. 3.4, see point 3.

4.3. On the selection of α for the explicit Robin-Neumann scheme

Two very interesting topics that are not yet discussed are: i) how to select not empirically a reasonable value of α that should fall in the range of stability and ii) which the dependence of the accuracy of explicit Robin-Neumann methods on α is. Here and in the next section we provide some preliminary answers to these two points.

A reasonable answer to question i) is to use for the explicit RN scheme the optimal value α_f^{opt} introduced to guarantee an efficient convergence of the implicit Robin-Neumann scheme, see Sect. 4.1. Since such

a value makes the convergence factor of the implicit method (thus the error at each iteraton) small, we expect that the use of the same value of α for the explicit counterpart of the method could reduce the error accumulated at each time step. Although this does not guarantee that the best value of α (in terms of accuracy of the explicit RN scheme) is achieved, it provides an effective way to obtain a value of α which is easily computable (see procedure reported in [19]), avoiding the manual investigation of several values of α.

We consider the same numerical experiment as above, with time discretization parameter $\Delta t = 0.001\,s$. In Figure 3, we report the mean pressure and displacement over the middle cross sections for $\alpha = \alpha_f^{opt} (= 1702)$, 1500, 2250, 3000.

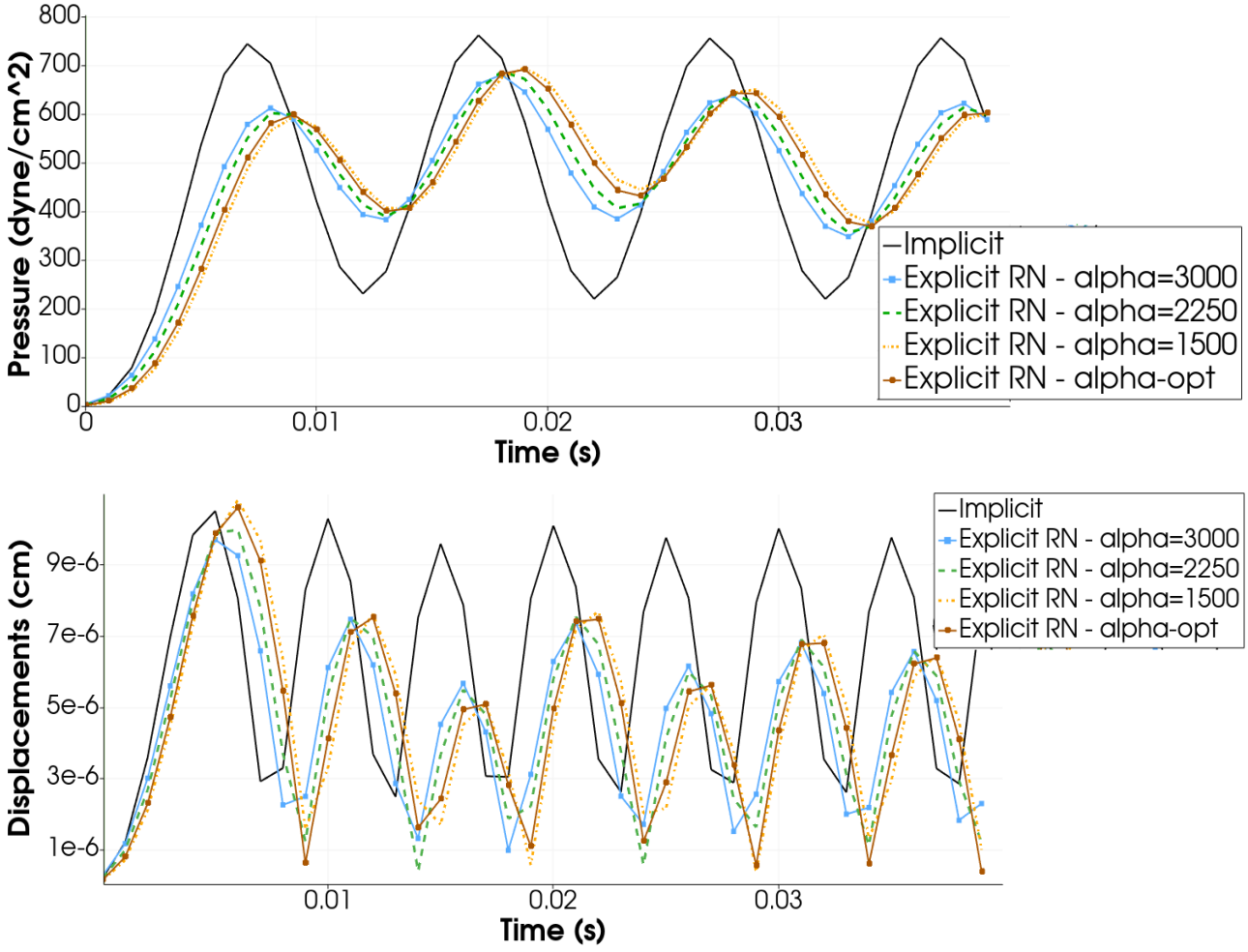

Figure 3: Fluid mean pressure (up) and structure mean displacement (bottom) over the middle cross section ($z = L/2 = 2.5\,cm$) for different values of α close to α_f^{opt}. Notice in black the solution obtained with an implicit method.

For $\alpha > 3500$ the solution blows up, whereas for $\alpha < 1500$ the accuracy deteriorates. We observe that the solution obtained with the value α_f^{opt} proposed a priori is very close to the optimal "manual" one ($\alpha = 3000$) found empirically (the latter intended as the most close to the implicit one). This result highlights that an effective a priori choice of α that guarantees stability and accuracy is possible, at least in the case of a cylindrical domain.

Remark 4.1. Notice that, from the computation of α_f^{opt} for decreasing values of Δt, we found that its value is greater than zero and does not blow up when $\Delta t \to 0$. Thus, from point 2 of the Discussion of Sect. 3.4, we have that $\delta \leq c(\alpha^{opt})^{-1}$ still makes sense also when $\Delta t \to 0$, since $\delta > 0$.

4.4. On the accuracy of the explicit Robin-Neumann scheme

Regarding issue ii) reported in the previous section, i.e. the accuracy of the explicit RN scheme, we present here numerical results obtained for mesh I and for different values of Δt, using the same data as above. In particular, in Figure 4 we report a comparison between the RN implicit and explicit solutions obtained both with α_f^{opt}. From these results, we observe that the two solutions, as expected, tend to coincide

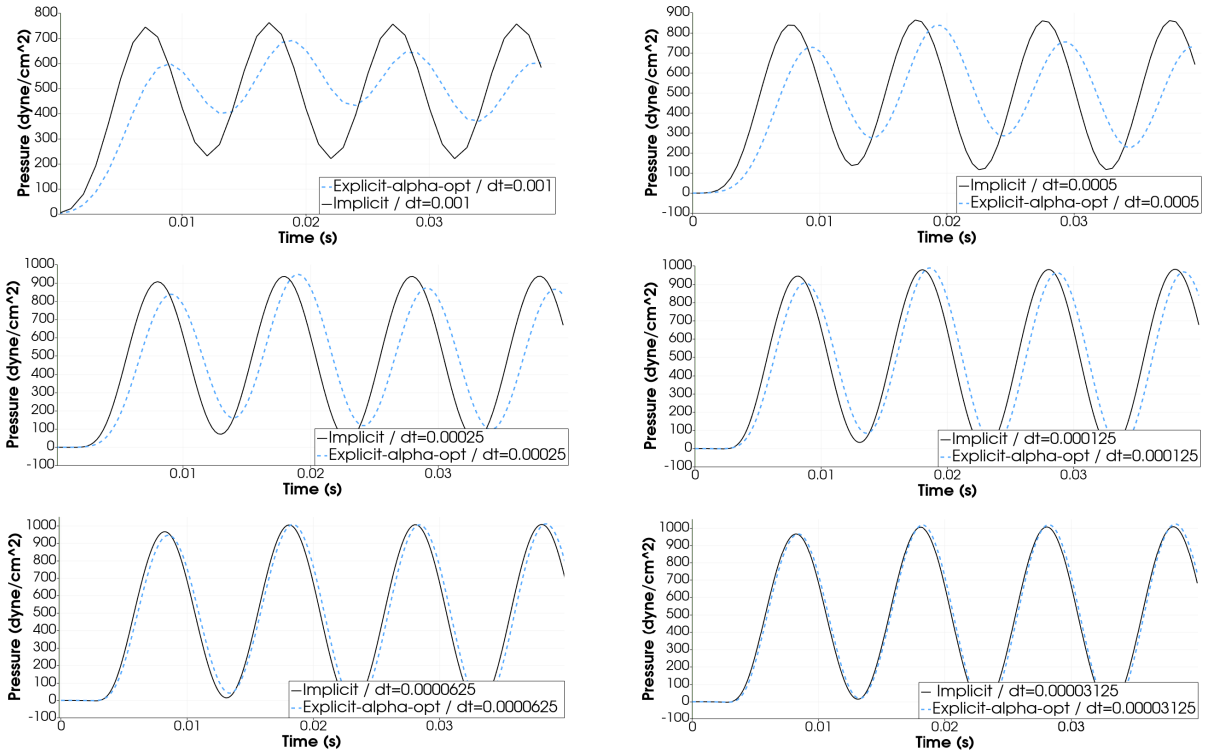

Figure 4: Comparison between the implicit RN and the explicit RN solutions for different values of Δt.

when Δt becomes smaller and smaller.

We also notice that the implicit solution reached experimental convergence (in the sense that the solution for smaller Δt did not change so much) for $\Delta t = \Delta t_1 = 0.000125$. On the other side, the explicit solution changed also for smaller values of Δt and only for $\Delta t = 0.00003125 = \Delta t_2 = \Delta t_1/4$ it seemed to have reached convergence. However, to obtain the implicit RN solution about 14 iterations (in average) per time step are required. This means that to go from t to $t + \Delta t_1$, we need to solve about 14 fluid and structure subproblems by using the implicit RN scheme, against 4 ($= \Delta t_2/\Delta t_1$) fluid and structure subproblems needed by the explicit RN scheme (which needs to solve only 1 fluid and structure subproblems per time step). This shows the reliability (at least for the proposed numerical experiment) of the explicit RN in terms of stability, accuracy and efficiency.

In order to go further towards the application of the explicit RN scheme to cases with physiological data, we present in what follows numerical results obtained by prescribing a physiological Dirichlet condition at the inlet of the cylindrical domain. This test aims at providing preliminary results towards the study of the reliability of the explicit Robin-Neumann scheme in real cases coming from hemodynamics. In particular, we consider the flow rate $X(t)$ depicted in figure 5, top, together with a parabolic velocity profile at each time step.

In Figure 5, bottom, we report the mean pressure over the middle cross section obtained for $\Delta t = 4 \cdot 10^{-3}$, both for the implicit and the explicit solutions obtained by the Robin-Neumann scheme. We observe a better agreement between implicit and explicit solutions (even with a larger value of Δt) with respect to the previous

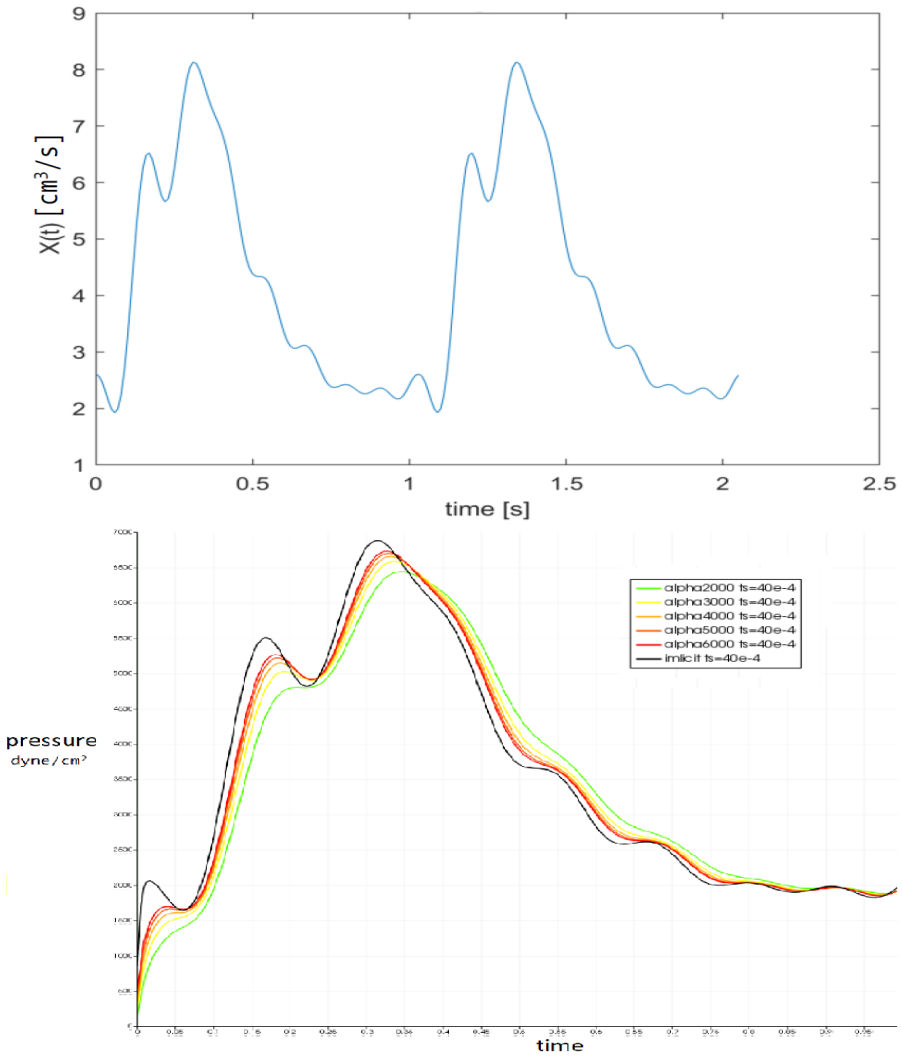

Figure 5: Up: Physiological flow rate prescribed at the inlet; Bottom: Fluid mean pressure over the middle cross section ($z = L/2 = 2.5\,cm$) obtained for the explcit RN scheme, for $\Delta t = 40 \cdot 10^{-4}$ and different values of α. Implicit solution in black.

test (see Figure 4). Probably, this is due to the smaller frequencies of the physiological signal with respect to $\cos\left(\frac{2\pi t}{0.01}\right)$. This is a very interesting result in view of clinical applications. This means that the explicit Robin-Neumann scheme seems to provide very accurate results with a decreased computational effort with respect to the implicit RN scheme, also in the case of a physiological input.

5. Conclusions

In this work we propose, for a model problem, an analysis of stability of a loosely-coupled scheme of Robin-Neumann type for the fluid-structure interaction problem, possibly featuring a large added mass effect. This allows us to find sufficient conditions for the value of the interface parameter α for both stability and instability solutions. In particular, the range of α guaranteeing stability becomes smaller for increasing added mass effect but it is not empty, indicating that also for a large added mass effect the loosely-coupled scheme is stable. Such a range increases its dimension for decreasing values of Δt, whereas for $h \to 0$ the stability properties worsen.

In order to make the results found in this paper reliable for concrete applications, we need now to apply them to realistic geometries and boundary data. This would make the explicit Robin-Neumann scheme an effective strategy to be considered for example in hemodynamics, where the added mass effect is elevated.

Acknowledgments

C. Vergara has been partially supported by the H2020-MSCA-ITN-2017, EU project 765374 "ROMSOC - Reduced Order Modelling, Simulation and Optimization of Coupled systems" and by the Italian research project MIUR PRIN17 2017AXL54F. "Modeling the heart across the scales: from cardiac cells to the whole organ". The authors would like also to thank the anonimous referees for their useful suggestions that allowed to improve the paper.

References

[1] Lifev user manual, `http://lifev.org`, 2010.

[2] M. Astorino, F. Chouly, and M. Fernández. Robin based semi-implicit coupling in fluid-structure interaction: stability analysis and numerics. *SIAM J. Sci. Comput.*, 31(6):4041–4065, 2009.

[3] S. Badia, F. Nobile, and C. Vergara. Fluid-structure partitioned procedures based on Robin transmission conditions. *J. Comput. Physics*, 227:7027–7051, 2008.

[4] S. Badia, F. Nobile, and C. Vergara. Robin-Robin preconditioned Krylov methods for fluid-structure interaction problems. *Comput. Methods Appl. Mech. Engrg.*, 198(33-36):2768–2784, 2009.

[5] S. Badia, A. Quaini, and A. Quarteroni. Splitting methods based on algebraic factorization for fluid-structure interaction. *SIAM J Sc Comp*, 30(4):1778–1805, 2008.

[6] J.W. Banks, W.D. Henshaw, and D.W. Schwendeman. An analysis of a new stable partitioned algorithm for fsi problems. part i: Incompressible flow and elastic solids. *J. Comput. Physics*, 269:108–137, 2014.

[7] M. Bukac, S. Canic, R. Glowinski, B. Muha, and A. Quaini. A modular, operator-splitting scheme for fluid–structure interaction problems with thick structures. *Int. J. Num. Meth. Fluids*, 74(8):577–604, 2014.

[8] M. Bukac, S. Canic, R. Glowinski, J. Tambaca, and A. Quaini. Fluid–structure interaction in blood flow capturing non-zero longitudinal structure displacement. *J. Comput. Physics*, 235:515–541, 2013.

[9] E. Burman and M.A. Fernández. Explicit strategies for incompressible fluid-structure interaction problems: Nitsche type mortaring versus robin–robin coupling. *Int. J. Num. Methods Engrg.*, 97:739–758, 2014.

[10] P. Causin, J.F. Gerbeau, and F. Nobile. Added-mass effect in the design of partitioned algorithms for fluid-structure problems. *Comput. Methods Appl. Mech. Engrg.*, 194(42-44):4506–4527, 2005.

[11] W.G. Dettmer, A. Lovric, C. Kadapa, and D. Peric. New iterative and staggered solution schemes for incompressible fluid-structure interaction based on dirichlet-neumann coupling. *Int. J. Num. Methods Engrg.*, pages 1 – 32, 2020.

[12] J. Donea. An arbitrary Lagrangian-Eulerian finite element method for transient dynamic fluid-structure interaction. *Comput. Methods Appl. Mech. Engrg.*, 33:689–723, 1982.

[13] C. Farhat, K.G. van der Zee, and P. Geuzaine. Provably second-order time-accurate loosely-coupled solution algorithms for transient nonlinear computational aeroelasticity. *Comput. Methods Appl. Mech. Engrg.*, 195:1973–2001, 2006.

[14] M. Fernandez, J. Mullaert, and M. Vidrascu. Explicit robin–neumann schemes for the coupling of incompressible fluids with thin-walled structures. *Comput. Methods Appl. Mech. Engrg.*, 267:566–593, 2013.

[15] M.A. Fernández. Incremental displacement-correction schemes for incompressible fluid-structure interaction - stability and convergence analysis. *Numerische Mathematik*, 123(1):21–65, 2013.

[16] M.A. Fernández, J.F. Gerbeau, and C. Grandmont. A projection semi-implicit scheme for the coupling of an elastic structure with an incompressible fluid. *Int. J. Num. Methods Engrg.*, 69(4):794–821, 2007.

[17] C. Forster, W. Wall, and E. Ramm. Artificial added mass instabilities in sequential staggered coupling of nonlinear structures and incompressible viscous flow. *Comput. Methods Appl. Mech. Engrg.*, 196(7):1278–1293, 2007.

[18] L. Gerardo Giorda, F. Nobile, and C. Vergara. Analysis and optimization of robin-robin partitioned procedures in fluid-structure interaction problems. *SIAM J. Numer. Anal.*, 48(6):2091–2116, 2010.

[19] G. Gigante and C. Vergara. Analysis and optimization of the generalized schwarz method for elliptic problems with application to fluid-structure interaction. *Numer. Math.*, 131(2):369–404, 2015.

[20] G. Guidoboni, R. Glowinski, N. Cavallini, and S. Canic. Stable loosely-coupled-type algorithm for fluid–structure interaction in blood flow. *J. Comput. Physics*, 228:6916–6937, 2009.

[21] K. Knopp. *Theory of functions: Parts I and II.* Dover Publications, 1996.

[22] M. Lukacova-Medvid'ova, G.Rusnakova, and A.Hundertmark-Zauskova. Kinematic splitting algorithm for fluid–structure interaction in hemodynamics. *Comput. Methods Appl. Mech. Engrg.*, 265:83–106, 2013.

[23] P. Moireau, N. Xiao, M. Astorino, C. A. Figueroa, D. Chapelle, C. A. Taylor, and J.F. Gerbeau. External tissue support and fluid–structure simulation in blood flows. *Biomechanics and Modeling in Mechanobiology*, 11(1–2):1–18, 2012.

[24] F. Nobile, M. Pozzoli, and C. Vergara. Time accurate partitioned algorithms for the solution of fluid-structure interaction problems in haemodynamics. *Computer & Fluids*, 86:470–482, 2013.

[25] F. Nobile, M. Pozzoli, and C. Vergara. Inexact accurate partitioned algorithms for fluid-structure interaction problems with finite elasticity in haemodynamics. *Journal of Computational Physics*, 273:598–617, 2014.

[26] F. Nobile and C. Vergara. An effective fluid-structure interaction formulation for vascular dynamics by generalized Robin conditions. *SIAM J Sc Comp*, 30(2):731–763, 2008.

[27] F. Nobile and C. Vergara. Partitioned algorithms for fluid-structure interaction problems in haemodynamics. *Milan Journal of Mathematics*, 80(2):443–467, 2012.

[28] K.C. Park, C.A. Felippa, and J.A. De Runtz. Stabilisation of staggered solution procedures for fluid-structure interaction analysis. *Comput. Methods Appl. Mech. Engrg.*, 26, 1977.

[29] S. Piperno and C. Farhat. Partitioned prodecures for the transient solution of coupled aeroelastic problems-Part II: energy transfer analysis and three-dimensional applications. *Comput. Methods Appl. Mech. Engrg.*, 190:3147–3170, 2001.

[30] A. Quarteroni, L. Dede', A. Manzoni, and C. Vergara. *Mathematical Modelling of the Human Cardiovascular System - Data, Numerical Approximation, Clinical Applications.* Cambridge University Press, 2019.

[31] A. Quarteroni, A. Manzoni, and C. Vergara. The cardiovascular system: Mathematical modelling, numerical algorithms and clinical applications. *Acta Numerica*, 26:365–590, 2017.

[32] A. Quarteroni, M. Tuveri, and A. Veneziani. Computational vascular fluid dynamics: Problems, models and methods. *Computing and Visualisation in Science*, 2:163–197, 2000.